Seeing Anderson localization

M. Hilke
Department of Physics, McGill University, Montréal, Canada H3A 2T8
(Received 10 January 2009; published 8 December 2009)

We propose an optical scheme to literally *see* Anderson localization by varying the optical wavelength or the angle of incidence in order to tune between localized and delocalized states in a random multilayered filter. This scheme allows us to clearly differentiate absorption from localization effects because the system behaves as a filter centered at a given wavelength, where only one wavelength is perfectly transmitted and all others are fully localized. At the resonant wavelength, the transmission is exactly one in the absence of absorption. The presence of absorption only changes the overall transmission but not the wavelength dependence. These results were obtained by developing a theoretical framework for the average optical transmission through disordered media.

DOI: 10.1103/PhysRevA.80.063820 PACS number(s): 42.25.Dd, 68.65.Ac

I. INTRODUCTION

Anderson localization was discovered about 50 years ago to describe the propagation of electrons in the presence of disorder [1]. The main prediction back then, was the existence of disorder induced localized states, which do not conduct electricity. Many years later it turns out, that the concept of Anderson localization is much more general and applies to almost any type of propagation in time or space, when more than one parameter is relevant (such as phase and amplitude). The occurrence of Anderson localization in the propagation of light, in particular, has become the focus of tremendous interest due to the emergence of new optical technologies and media such as low-dimensional and disordered optical lattices [2,3]. While several experiments have reported the measurement of Anderson localization of light [2–9], many of the observations remain controversial because the effects of absorption and localization have a similar signature, i.e., exponential decrease in the transmission with the system size [10,11].

In order to literally *see* Anderson localization and to distinguish it from absorption, we consider the system shown in Fig. 1. The setup is composed of N_f filters in series. Each filter is composed of N_l random optical layers and each layer has a refractive index n_j and a thickness d_j as defined in Fig. 2. For optimal results, it is important that these layers are very well defined. This is possible, for instance, by using high accuracy multilayer growth techniques such as molecular beam epitaxy (MBE). Good material choices include large band gap materials such as GaN ($\Delta=3.2$ eV, $n \simeq 2.3$) and InN ($\Delta=2$ eV, $n \simeq 3.1$), which can be grown by MBE with atomic precision [12,13]. The absence of surface roughness ensures that this multilayered system is one-dimensional in nature. Important surface roughness would induce scattering at stray angles, which can lead to a one-dimensional (1D) to three-dimensional (3D) crossover [14], thereby strongly reducing localization effects, since localization in 3D is much weaker than in 1D [15] and therefore much more challenging to observe [8].

To illustrate the general behavior of our system, we considered the simplest random system of a binary distribution, where we assume two kinds of materials, one with a refraction index of $n_0=1$ and the other with $n_1=3$. Adding more materials will not change the results qualitatively and the analytical expressions derived below remain valid for any choice or combination of materials.

The filters are placed in a way to allow the insertion of a grating between any of them. The grating is necessary to resolve the spectral composition of the transmitted light. The position of the grating can be changed in order to measure the transmission after $1,2,\ldots,$ or N_f filters in series. When using a white light source, this allows to spectrally resolve the transmission after any number of filters. Anderson localization will then lead to an exponential decay of the transmission with the number of filters (see Fig. 1).

A. Fluctuations

A major difficulty in observing Anderson localization is the existence of strong fluctuations [11,16]. In general, the relative fluctuations of the transmission ($\delta T/\langle T\rangle$) diverge with decreasing transmission, where $\delta T=\sqrt{(T-\langle T\rangle)^2}$ and $\langle T\rangle$ is the average transmission. This is a fundamental problem, which can be circumvented by considering $\ln(T)$ (the transmission in decibel) or the inverse transmission since in both cases the relative fluctuations decrease with decreasing transmission as shown in Fig. 2 for $\ln(T)$ and is equivalent to a configurational average. Such a log average over a small number of configurations is feasible experimentally, since it simply involves averaging the signal in decibel over several configurations, corresponding to exchanging the position of some filters. The numerical examples shown in the middle of Fig. 1 are based on a small log average over 100 configurations and assuming 100 different filters, each with an average of 50 random layers and a spectral resolution of 1nm. The two bottom graphs are obtained by numerically averaging the transmission over 100 random layers directly, whereas the curves without absorption ($\kappa=0$) and without surface roughness ($\sigma=0$) are obtained using the analytical expression from Eq. (3). The small fluctuations for κ and σ small are due to the finite size effects of the numerical solution.

B. Numerical approach

The numerical results were obtained using a standard method to describe a multilayered optical system with a

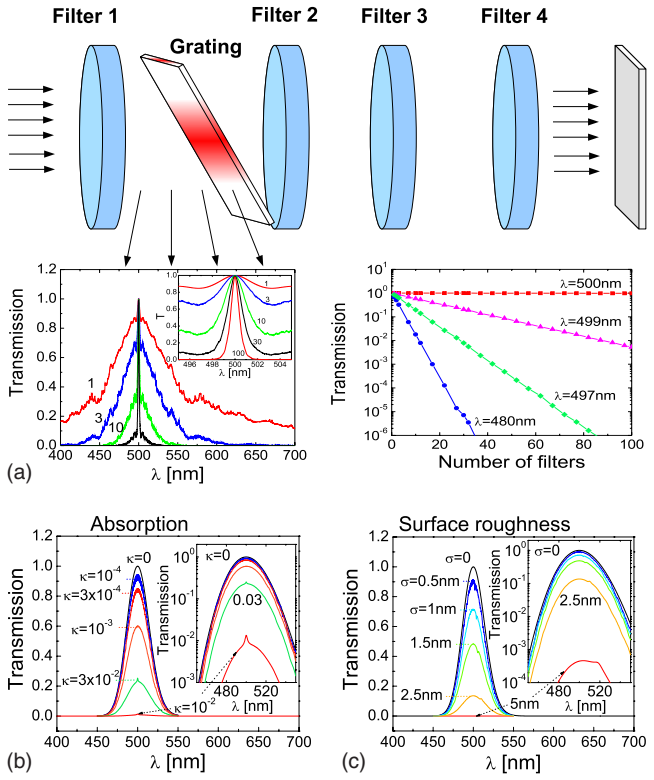

FIG. 1. (Color online) The top shows the arrangement of the filters, where a grating can be inserted in order to measure the wavelength dependence of the transmission. The transmission is shown in the middle left figure when the grating is placed after 1, 3, 10, 30, or 100 filters, which increases the quality factor filter with the number of layers. The middle right figure represents the dependence of the transmission on the number of layers at several wavelengths (480, 497, 499, and 500) nm, indicating an exponential decay. The bottom left and right figures show the average transmission through 100 random layers for different values of absorption and surface roughness, respectively.

transfer matrix. Each matrix describes the transmission after one layer, where we assume the layers to be normal to the $\hat{x}$ direction. For transverse magnetic (TM) waves, where the magnetic-field component H^z is parallel to each layer and the electric field component E^y is at an angle θ (the angle of incidence) to the first layer, the transfer matrix can be written as [17]:

$$\begin{pmatrix} H_{j-1}^z \\ E_{j-1}^y \end{pmatrix} = \underbrace{\begin{pmatrix} \cos(\phi_j) & -i\sin(\phi_j)/\gamma_j \\ -i\sin(\phi_j)\gamma_j & \cos(\phi_j) \end{pmatrix}}_{M_j} \begin{pmatrix} H_j^z \\ E_j^y \end{pmatrix}, \tag{1}$$

For an incoming wave of wavelength λ, the field components on one side of a stack of N_l layers can therefore be related to the fields on the other side by taking the product of the transfer matrices ($M=\prod_{j=1}^{N_l} M_j$). Assuming a vacuum impedance z_0 before and after the filter, the transmission of light is given by $T=4|M_{11}+\gamma M_{12}+M_{21}/\gamma+M_{22}|^{-2}$, where M_{kl} are the matrix elements of M [17]. The matrix elements of M_j used in Eq. (1) are material dependent with $\phi_j=(2\pi d_j/\lambda)\sqrt{n_j^2-\sin^2(\theta)}$ and $\gamma_j=(z_0/n_j^2)\sqrt{n_j^2-\sin^2(\theta)}$. For

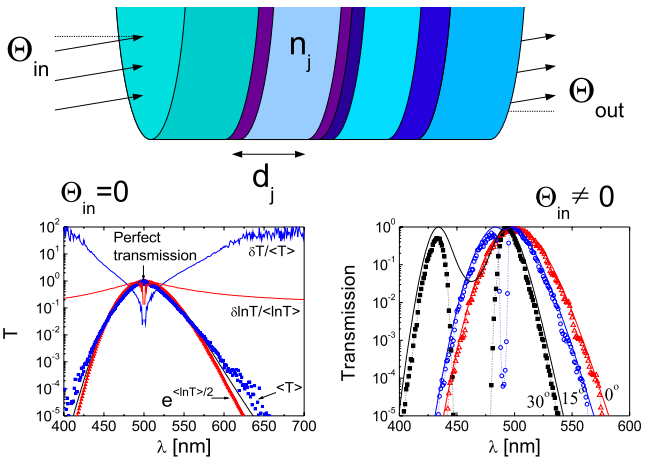

FIG. 2. (Color online) The top picture illustrates the details of a random sequence of layers composing one filter. In the bottom left figure the transmission as a function of wavelength is shown for a system of 200 layers averaged 10^4 times. The analytical result from Eq. (3) is shown with a continuous line. The numerical average and relative fluctuations are shown with square and triangles. The transmission as a function of wavelength for different incidence angles (0, 15, and 30°) is depicted in the bottom right figure, where the continuous lines correspond to the analytical expression (3), whereas the dotted lines correspond to the numerical log average.

transverse electrical (TE) waves these expressions have to be replaced by $H^z \to E^z$, $E^y \to -H^y$, and $\gamma_j=z_0^{-1}\sqrt{n_j^2-\sin^2(\theta)}$.

C. Absorption

A major roadblock in the observation of Anderson localization is the presence of absorption. Absorption stems from the imaginary part of the refraction index, κ_j, where $n_j=n_j^r+i\kappa_j$. n_j^r is the real part and the imaginary component κ_j is large when photon energies approach the band-gap energy or when the materials are conducting. For the numerical calculations, the expressions above remain valid even if n_j has a complex part (leading to complex angles). Remarkably, the presence of absorption does not significantly alter the localization-delocalization transition (LDT), which is still observed for reasonable values of absorption as shown in Fig. 1 (graph absorption). While the overall transmission is strongly reduced for values of $\kappa_j \simeq 10^{-2}$ for each layer, the relative wavelength dependence is not affected. Hence, even in the presence of absorption we can observe the LDT discussed below.

D. Surface roughness

Another potential issue is the presence of surface roughness between two adjacent layers. This can be modeled by inserting a layer of width $d=2\sigma$, where σ is the surface root mean square and the corresponding refractive index is $n=\sqrt{(1+n_j^2)/2}+i\pi d(n_j-1)^2/(2\sqrt{2}\lambda)$ [18]. This approach is valid when the correlation length of the roughness is much smaller than the wavelength. In Fig. 1 (surface roughness) we show that a small surface roughness does not signifi-

cantly affect the LDT, which is the key to observing Anderson localization.

E. Localization delocalization transition

The LDT is obtained under the following condition: For a given layer there exists a set of thicknesses $d_j = m\lambda_0/2n_j$ (m any integer) for which the layer is totally transparent at normal incidence and for the resonant wavelength λ_0. This corresponds to $\sin(\phi_j)=0$ and to M_j equal to the identity matrix and does not depend on the neighboring layers. When randomly combining different layers with the same resonance condition, the overall resonance condition is preserved. The position of these resonances was discussed by Cristanti [19]. Away from the resonant wavelength the system behaves like a random system leading to Anderson localization. This type of disorder was also studied in the context of electronic transport in 1D and two-dimensional (2D) [20–22], where metal-insulator type transitions were found. Figures 1 and 2 show this resonance, where the transmission is one (transparent) at $\lambda_0=500$ nm and then decreases exponentially ($T \simeq e^{-K(\lambda-\lambda_0)^2}$) away from the resonance condition. K is a form factor which is proportional to the number of random layers and also depends on the variance of the disorder as discussed below. This dependence on the number of layers can then be used to tune the quality factor of the filter. Without this special resonance condition, the transmission through random optical layers decays exponentially at all wavelengths at a similar rate [9,23,24]. The LDT implies that this decay is dependent on the wavelength even in the presence of absorption.

F. Analytical approach

We now turn to characterize the transmission through this random system by evaluating the product of M_j's composed of random elements. Similar products of random matrices have been widely studied and lead to matrix elements, which increase exponentially with the number of products. The rate of this exponential dependence is termed the Lyapunov exponent and will be derived analytically below. The Lyapunov exponent corresponds to the inverse of the localization length, beyond which the transmission vanishes. To obtain analytical results the trick is to consider the square of the fields, $|H_j^z|^2$ instead of H_j^z. This allows to capture the dominant behavior beyond the plane-wave oscillations. A similar technique was actually used in the context of electronic transport [25–27] and we extend it here to optical systems. Squaring Eq. (1) then leads to the following iterative equation:

$$\underbrace{\begin{pmatrix} |H_{j-1}^z|^2 \\ |E_{j-1}^y|^2 \\ 2\Im\{H_{j-1}^z (E_{j-1}^y)^*\} \end{pmatrix}}_{\vec{F}_{j-1}} = \underbrace{\begin{pmatrix} \cos^2(\phi_j) & (\sin(\phi_j)/\gamma_j)^2 & i\cos(\phi_j)\sin(\phi_j)/\gamma_j \\ (\sin(\phi_j)\gamma_j)^2 & \cos^2(\phi_j) & -i\cos(\phi_j)\sin(\phi_j)\gamma_j \\ 0 & 0 & \cos^2(\phi_j)-\sin^2(\phi_j) \end{pmatrix}}_{M_j^{3\times 3}} \underbrace{\begin{pmatrix} |H_j^z|^2 \\ |E_j^y|^2 \\ 2\Im\{(H_j^z (E_j^y)^*\} \end{pmatrix}}_{\vec{F}_j}. \tag{2}$$

For N_l layers, the total transmission is now determined by the product $\vec{F}_0 = (\Pi_{j=1}^{N_l} M_j^{3\times 3})\vec{F}_{N_l}$, which can be averaged over the disorder, leading to, $\langle \vec{F}_0 \rangle = \langle M^{3\times 3} \rangle^{N_l} \langle \vec{F}_{N_l} \rangle$, where $\langle M^{3\times 3} \rangle$ is the disorder average of $M_j^{3\times 3}$ assuming that the material parameters of the layers are not correlated. The disorder average depends on the distribution of the parameters entering $M_j^{3\times 3}$. The leading behavior is obtained by taking the eigenvalues of $\langle M^{3\times 3} \rangle$, from which the Lyapunov exponent can be extracted as $\Lambda = \max\{\ln|\mathrm{Eig}(\langle M^{3\times 3} \rangle)|\}$. This yields an expression for the average resistance (inverse transmission), where $\langle 1/T \rangle = e^{\Lambda N_l}$. Hence, perfect transmission corresponds to the case where $\Lambda=0$. Interestingly, this expression can also be related to the log-average transmission $\langle \ln T \rangle = -\Lambda N_l/2$ and to the average transmission $\langle T \rangle = e^{-\Lambda N_l/4}$, where the factors of 1/2 stem from the properties of the distribution of T's [26]. The next step is obtaining $\langle M^{3\times 3} \rangle$ for a given distribution. For discrete distributions such as the binary one this is quite straightforward, since the layer properties are determined by only two possible configurations, $\{d_0, n_0\}$ and $\{d_1, n_1\}$, respectively. This yields

$$\langle M^{3\times 3} \rangle = (M_0^{3\times 3} + M_1^{3\times 3})/2, \tag{3}$$

where $M_0^{3\times 3}$ and $M_1^{3\times 3}$ are simply $M_j^{3\times 3}$ with $\{d_j = d_0,\ n_j = n_0\}$ and $\{d_j = d_1,\ n_j = n_1\}$, respectively. For continuous distributions, analytical expressions for $\langle M^{3\times 3} \rangle$ are often too complicated to be useful and can be instead integrated numerically.

Comparing these analytical expressions to the numerical results demonstrate a remarkable agreement as seen in Figs. 1 and 2. The analytical expression using Eq. (3) reproduces all the main features and shows the resonance behavior at $\lambda=\lambda_0$. The analytical expression is extremely useful in situations, where the localization length is large, since its numerical determination would require a system size exceeding the localization length as well as configurational averaging, which can be computationally very expensive. Moreover, our analytical expression (3) also works very well close to the resonance, which gives $\Lambda \sim (\lambda-\lambda_0)^2$ and perfectly reproduces our numerical results. This determines the form factor K, which depends on the variance of the disorder. (Zero variance leads to $K=0$ or $\Lambda=0$.) Deviations exist when looking

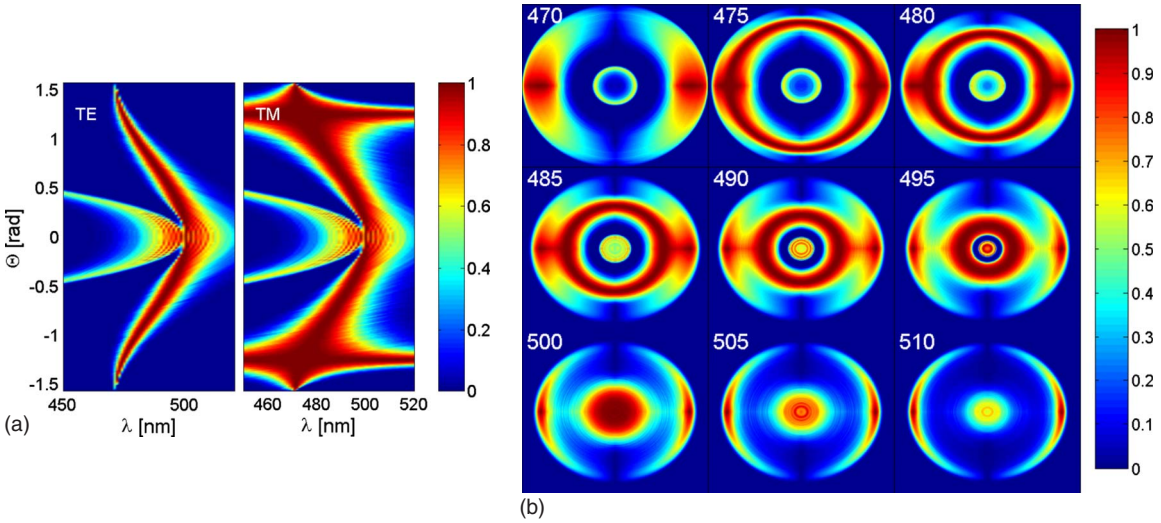

FIG. 3. (Color online) Left: The wavelength and incidence angle dependence of the transmission through a random multilayer on a linear color scale for TE waves (left) and TM waves (right). Right: The transmission is shown on a linear color scale as a function of the angle of incidence in the $\hat{y}$ and $\hat{z}$ directions. Each subgraph spans $-\pi/2$ to $+\pi/2$ and corresponds to a different wavelength. The resonant wavelength ($\lambda_0=500$ nm) corresponds to the bottom left panel. The horizontal (vertical) axis would correspond to the angle dependence of a TM (TE) wave.

at the angle dependence, as shown in Fig. 2. While the analytical expression predicts two transmission peaks with a weak minimum in between, the numerical results show that the minimum is more pronounced. This can be attributed to restricting the average to the second moment, which can lead to differences with the numerical results and in some cases even lead to fluctuations in the Lyapunov exponent [27].

G. Angle dependence

Quite remarkably, it is now possible to tune the wavelength of the resonance, simply by tilting the filter. We present the angle and wavelength dependence of the transmission in Fig. 3 for both the TE and TM waves using 200 random layers averaged over 100 configurations. Two branches can be observed, one which is perfectly transmitting and a second one which vanishes with increased angle. In addition, there is an angle $\Theta \simeq \pm 1.25$ with perfect transmission for the TM incidence, where $\Theta=\arctan(n_1/n_0)$ rad and $n_1/n_0=3$ for our particular configuration. This angle corresponds to the Brewster angle.

By combining the expression for TE and TM waves it is possible to obtain the results for any polarization, simply by using a linear combination of TE and TM waves. Moreover, we can analyze what happens when tilting the filter in one or the other direction. The tilt angle can be varied in two spatial directions, one corresponding to the TM direction and the other to the TE direction, or a combination of both, which is seen in Fig. 3. Perfect transmission is now identified in a form of a ring, whose diameter depends on the wavelength. This angular dependence therefore allows for a direct and beautiful visualization of the LDT and hence localization of the averaged transmission.

Summarizing, we have shown a filter design, where we can directly visualize Anderson localization by using a LDT. The filter design is *perfect* in the sense that only one visible wavelength is transmitted perfectly and all others are exponentially suppressed. Not only does this provide for an optimal filter design but also allows us to *see* Anderson localization 50 years after its discovery.

The author acknowledges financial support from NSERC, FQRNT, RQMP and INTRIQ.

[1] P. W. Anderson, Phys. Rev. **109**, 1492 (1958).
[2] T. Schwartz, G. Bartal, S. Fishman, and M. Segev, Nature (London) **446**, 52 (2007).
[3] Y. Lahini, A. Avidan, F. Pozzi, M. Sorel, R. Morandotti, D. N. Christodoulides, and Y. Silberberg, Phys. Rev. Lett. **100**, 013906 (2008).
[4] D. S. Wiersma, P. Bartolini, A. Lagendijk, and R. Righini, Nature **390**, 671 (1997).
[5] J. Bertolotti, S. Gottardo, D. S. Wiersma, M. Ghulinyan, and L. Pavesi, Phys. Rev. Lett. **94**, 113903 (2005).
[6] K. Y. Bliokh, Y. P. Bliokh, V. Freilikher, A. Z. Genack, B. Hu, and P. Sebbah, Phys. Rev. Lett. **97**, 243904 (2006).
[7] K. Y. Bliokh, Y. P. Bliokh, V. Freilikher, A. Z. Genack, and P. Sebbah, Phys. Rev. Lett. **101**, 133901 (2008).
[8] M. Störzer, P. Gross, C. M. Aegerter, and G. Maret, Phys. Rev. Lett. **96**, 063904 (2006).
[9] M. V. Berry and S. Klein, Eur. J. Phys. **18**, 222 (1997).
[10] F. Scheffold, R. Lenke, R. Tweer, and G. Maret, Nature (Lon-

don) **398**, 206 (1999).
[11] A. A. Chabanov, M. Stoytchev, and A. Z. Genack, Nature (London) **404**, 850 (2000).
[12] F. A. Ponce and D. P. Bour, Nature (London) **386**, 351 (1997).
[13] A. Khan, K. Balakrishnan, and T. Katona, Nat. Photonics **2**, 77 (2008).
[14] S. Zhang, J. Park, V. Milner, and A. Z. Genack, Phys. Rev. Lett. **101**, 183901 (2008).
[15] E. Abrahams, P. W. Anderson, D. C. Licciardello, and T. V. Ramakrishnan, Phys. Rev. Lett. **42**, 673 (1979).
[16] A. Z. Genack and A. A. Chabanov, J. Phys. A **38**, 10465 (2005).
[17] J. Chilwell and I. Hodgkinson, J. Opt. Soc. Am. A **1**, 742 (1984).
[18] C. K. Carniglia and D. G. Jensen, Appl. Opt. **41**, 3167 (2002).
[19] A. Crisanti, J. Phys. A **23**, 5235 (1990).
[20] J. C. Flores, J. Phys.: Condens. Matter **1**, 8471 (1989).
[21] D. H. Dunlap, H.-L. Wu, and P. W. Phillips, Phys. Rev. Lett. **65**, 88 (1990).
[22] M. Hilke, Phys. Rev. Lett. **91**, 226403 (2003).
[23] K. Yu. Bliokh and V. D. Freilikher, Phys. Rev. B **70**, 245121 (2004).
[24] S. Caracciolo and A. D. Sokal, J. Phys. A **19**, L797 (1986).
[25] P. Erdös and R. C. Herndon, Adv. Phys. **31**, 65 (1982).
[26] J. B. Pendry, Adv. Phys. **43**, 461 (1994).
[27] M. Hilke, Phys. Rev. B **78**, 012204 (2008).